GBE

Ancestral Chromosome-Level Assemblies Reveal Posthybridization Genome Evolution in the New Mexico Whiptail Lizard (*Aspidoscelis neomexicanus*)

David V. Ho [1,2,†], Aaron Odell [1,†], Duncan Tormey [3], Nathaniel Deimler [1,2], Valentine Patterson[1], Dai Tsuchiya [3], Randy L. Klabacka [4,5], Robert R. Schnittker[3], Diana P. Baumann[3], William B. Neaves[3], Anthony J. Barley [6], Peter Baumann [1,2,7,*]

[1]Department of Biology, Johannes Gutenberg University, Mainz 55128, Germany

[2]Institute for Quantitative and Computational Biosciences, Johannes Gutenberg University, Mainz 55128, Germany

[3]Stowers Institute for Medical Research, Kansas City, MO 64110, USA

[4]Department of Biological Sciences and Museum of Natural History, Auburn University, Auburn, AL 36849, USA

[5]Department of Biology, Brigham Young University, Provo, UT 84602, USA

[6]School of Mathematical and Natural Sciences, Arizona State University, Glendale, AZ 85306, USA

[7]Institute of Molecular Biology, Mainz 55128, Germany

*Corresponding author: E-mail: peter@baumannlab.org.

[†]David V. Ho and Aaron Odell contributed equally to this work.

Accepted: November 13, 2025

Abstract

Unisexual species of whiptail lizards in the genus *Aspidoscelis* arose by interspecific hybridization. They reproduce clonally through parthenogenesis and are thought to maintain the fixed heterozygosity that resulted from their hybrid origin by avoiding recombination between homeologous chromosomes. In the absence of chromosome-level assemblies for the sexual progenitor species, questions relating to the long-term consequences of clonal reproduction have remained largely unanswered. Here, we present chromosome-level genome assemblies for *A. marmoratus* and *A. arizonae*, the parental species of the unisexual *A. neomexicanus*. Using these references, we have analyzed whole-genome sequencing data from both wild and laboratory-reared *A. neomexicanus* individuals as well as newly generated F_1 hybrids. Our analysis identified population-specific losses of heterozygosity affecting multiple syntenic chromosome pairs, demonstrating that homeologous chromosome pairing and recombination must occur at a low frequency and contribute to genome erosion in these unisexual lineages. The loss of heterozygosity patterns we observed further suggest that the genomes of unisexual lineages diverge over time more quickly than anticipated based on mutation accumulation alone. Our results establish genomic resources for *Aspidoscelis* and provide new insights into how genome structure can evolve in the absence of sexual reproduction.

Key words: reference genome, *Aspidoscelis arizonae*, *Aspidoscelis marmoratus*, parthenogenesis, loss of heterozygosity, squamate.

Significance

Chromosome-level genome assemblies for *Aspidoscelis marmoratus* and *A. arizonae* represent the first high-quality genomic resources for this genus and provide a foundation for investigating evolutionary processes in both sexual and unisexual species. As a test case for the usefulness of these reference genomes, we show that the unisexual *A. neomexicanus* (a hybrid with origins between *A. marmoratus* × *A. arizonae*) exhibits population-specific genomic divergence resulting from loss of heterozygosity, challenging the assumption that clonal reproduction preserves long-term heterozygosity genome-wide.

Introduction

Squamates, the order encompassing lizards and snakes, represent one of the most diverse and ecologically widespread groups of vertebrates, with over 11,900 recognized species (Uetz et al. 2025). Yet, despite their diversity and evolutionary significance as a highly diverse clade within amniotes, squamates remain deeply underrepresented in genomic databases (Hotaling et al. 2021), particularly when it comes to chromosome-level genome assemblies. This dearth in resources limits our ability to investigate fundamental questions about genome evolution, chromosome structure, and the mechanisms underlying diversity in a number of life history traits within this group.

Among squamates, the genus *Aspidoscelis* (formerly part of *Cnemidophorus*, family Teiidae) (Reeder et al. 2002) is particularly notable for its reproductive biology, as the genus includes both sexual and multiple independently derived unisexual species that are comprised entirely of female individuals. This group of lizards represents the highest diversity of unisexual lineages among vertebrates (>30 sexual species and ∼15 recognized unisexual species) (Reeder et al. 2002). Hybridization between sexual *Aspidoscelis* species is common and has resulted in a complex pattern of introgression while mostly maintaining gonochorism (Reeder et al. 2002; Barley et al. 2022). In rare instances, diploid unisexuals arose through hybridization between sexual species, when a first-generation hybrid acquired the ability to reproduce clonally through parthenogenesis (Lowe and Wright 1966; Neaves 1969; Lutes et al. 2010). Rare secondary hybridization events between these diploid unisexual females and sexual males of related species can produce unisexual triploids (Pennock 1965; Walker et al. 1997), and tertiary hybridization events results in tetraploid lineages (Neaves 1971; Lutes et al. 2011) While specimens representing various diploid and triploid parthenogenetic species are common in much of the southwestern United States, tetraploid individuals have rarely been reported in nature, but are readily produced in captivity where they have been propagated for up to nine generations thus far (Lutes et al. 2011; Cole et al. 2014, 2017, 2023). Among the sexual species, incidences of facultative parthenogenesis (which differs mechanistically from obligate parthenogenesis) have been described to occur even in the presence of males in *A. marmoratus* and *A. arizonae* (Ho et al. 2024). This diversity in reproductive mechanisms makes *Aspidoscelis* a compelling system for investigating how different forms of reproduction influence genetics, evolution, and the longevity of species.

Thus far, much of what we know about the evolution and maintenance of sexual and unisexual *Aspidoscelis* species has come from allozyme analysis, skin grafting, microsatellite analysis, reduced representation sequencing, cytogenetics, and microscopy (Cuellar and McKinney 1976; Cole et al. 1988; Reeder et al. 2002; Lutes et al. 2010, 2011; Newton et al. 2016; Barley et al. 2019; Persons et al. 2021). These approaches have provided foundational insights into the consequences of hybridization, hybrid origins of unisexual lineages, and the long-term preservation of heterozygosity within unisexual lineages. However, these studies did not address whether heterozygosity is maintained long-term and genome-wide. This question became particularly pertinent to ask in light of recent reports of loss of heterozygosity (LOH) in stick insects and other parthenogenetic species (Jaron et al. 2021, 2022; Simion et al. 2021; Lv et al. 2025). The recent integration of cytological and computational methods to produce a reference genome for *A. marmoratus* identified a postmeiotic genome duplication as the mechanism enabling facultative parthenogenesis in whiptail lizards, resulting in a genome-wide LOH (Ho et al. 2024). This underscores the importance of genome assemblies for addressing fundamental questions such as genome-wide patterns of recombination, structural variations, the extent and mechanisms of LOH, and the rate of genomic decay in parthenogenetic lineages.

To further address this resource gap, we have elevated the previously published assembly for the Marbled Whiptail *A. marmoratus* (Ho et al. 2024; Fig. 1a) to chromosome-level resolution and generated a chromosome-level genome assembly for the Arizona Striped Whiptail *A. arizonae* (Fig. 1b). The two species are phenotypically well separated (Fig. 1c) and belong to different *Aspidoscelis* clades, with *A. marmoratus* being part of the *tigris* group and *A. arizonae* being part of the *inornatus* complex (Reeder et al. 2002) (Fig. 1d). Here, we first present the genome assemblies for *A. marmoratus* and *A. arizonae*, including metrics of

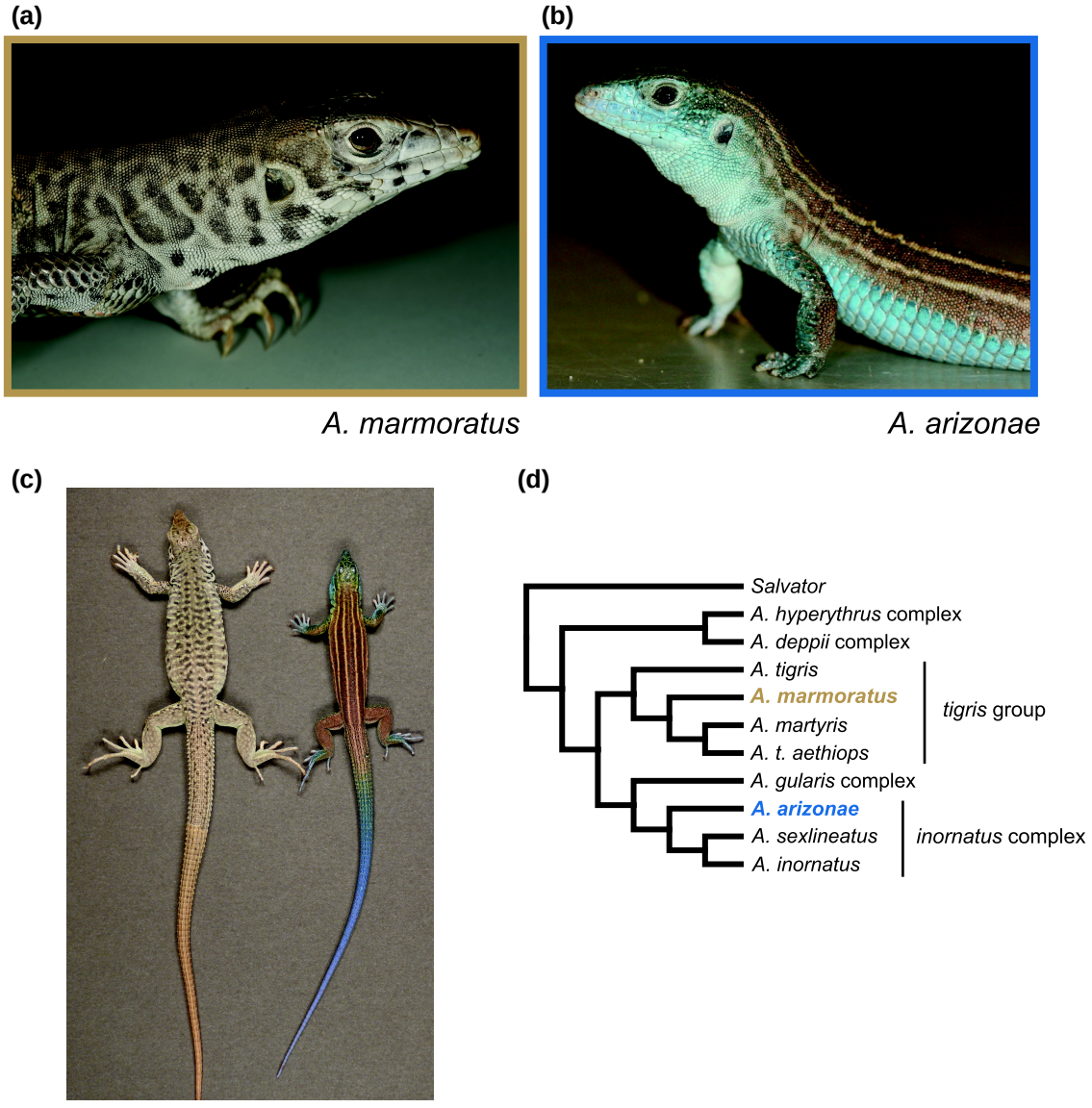

Fig. 1. Focal species and phylogenetic context within the genus *Aspidoscelis*. a) *Aspidoscelis marmoratus*, a member of the *tigris* group, characterized by light and dark reticulated pattern on dorsum. b) *Aspidoscelis arizonae*, a member of the *inornatus* complex, characterized by stripes on the dorsum and blue ventral coloration. c) Dorsal view *A. marmoratus* (left) and *A. arizonae* (right). d) Cladogram illustrating the phylogenetic relationships among major lineages within *Aspidoscelis* based on previously published analyses (Barley et al. 2022). Note placement of the *A. marmoratus* (brown) within the *tigris group* and *A. arizonae* (blue) within the *inornatus* complex. The outgroup is *Salvator merianae*, another member of the Teiidae family.

assembly quality and validation. We then compare their genome structures, identify the fusion events underlying their convergent karyotypes, and annotate genic and repetitive content. As *A. marmoratus* and *A. arizonae* are the parental species of the unisexual *A. neomexicanus* (Cole et al. 1988), we applied whole-genome sequencing to newly generated F_1 hybrids, as well as individuals of *A. neomexicanus* collected in different natural populations or raised for up to eight generations in our laboratory colony. Anchoring a genomic analysis to both parental genomes revealed distinct patterns of LOH that distinguish populations of what has thus far been considered a clonal species derived from a single, historical hybridization event.

Results

Sequencing and Assembly of the *A. marmoratus* and *A. arizonae* Genomes

A chromosome-level genome assembly of *A. marmoratus* was generated utilizing Hi-C data and the proprietary HiRise scaffolding pipeline from Dovetail Genomics, which leverages three-dimensional chromatin contact maps to

order and orient contigs. The Hi-C libraries were constructed from the same individual as the first AspMar1.0 assembly (Ho et al. 2024), which consisted of 3,826 scaffolds, a scaffold N50 length of 32.2 Mb, and a total haploid genome size of 1.639 Gb. Prior to scaffolding with the Hi-C data, a misjoin was identified on scaffold Scpiza6a_72 (42,780,895 bp) that was subsequently split into two scaffolds (positions 1 to 37,005,007 and positions 37,005,008 to 42,780,895). Following de novo scaffolding of the previous AspMar1.0 assembly, the resulting assembly had 3,519 scaffolds, with an improved scaffold N50 length of 113 Mb, corresponding to the fifth largest scaffold (Fig. 2a). While the absolute number of scaffolds only decreased by 8% between the two assemblies, the proportion of the genome represented by the 23 largest scaffolds increased from 65.36% in the first assembly to 99% in the second assembly (Fig. 2b), while the remaining unincorporated scaffolds represent small fragments. The twenty-three large scaffolds correspond to the number of chromosomes observed in historical karyotype data for this species (Lowe and Wright 1966; Cole et al. 1988), and the relative scaffold sizes correlate well with three macrochromosomes (>150 Mb), eight mid-sized chromosomes (50 to 150 Mb), and 12 microchromosomes (<50 Mb). These observations strongly support that we have generated a chromosome-level assembly for *A. marmoratus*.

To independently verify this assembly, we developed a custom computational genome assembly pipeline designed specifically to leverage Hi-C proximity-ligation sequencing data. This Genome Assembly Booster (GAB) constitutes a scaffolding method (see Methods and Supplemental Methods) and is dependent on the existence of a primary genome assembly and Hi-C data (Fig. S1A). The GAB algorithm largely confirmed the earlier chromosome-scale assembly for *A. marmoratus* with comparable clustering of scaffolds into chromosome-level groups (Fig. S2A and S2B). These results validated the new methodology and built confidence in the original assembly, which was then used for subsequent analyses described below. To further evaluate the *A. marmoratus* assembly, we visualized Hi-C contact maps for each of the 23 chromosomes and observed the presence of strong intrachromosomal contact patterns with no obvious assembly errors (Fig. S2C). To further test the accuracy of the *A. marmoratus* assembly, we performed single-chromosome sequencing on the three largest chromosomes. Four sequencing libraries were generated: one from a single isolated chromosome 1, and three from pools of isolated chromosomes (12 chromosome 1s, nine chromosome 2s, and 11 chromosome 3s). Reads from each library were mapped back to the reference genome, and each showed highly specific alignment to the corresponding chromosome (Fig. S3A). Coverage profiles across the chromosomes were uniform and continuous, consistent with high assembly contiguity and completeness (Fig. S3B). Taken together, these results provide independent validation of the *A. marmoratus* genome assembly.

Next, we applied the GAB to sequencing data for *A. arizonae*, where a wild-caught male *A. arizonae* (ID 17121) collected near Alamogordo, New Mexico, USA, served as the source material for genomic DNA isolation. To help guide our expectation regarding genome size, k-mer counts from short-read Illumina data were passed through GenomeScope2.0 (Ranallo-Benavidez et al. 2020), yielding an estimated haploid genome size of 1.47 Gb (Fig. S4). A primary assembly was generated at Dovetail Genomics using a combination of Illumina short-read and Chicago libraries. This assembly comprised of 3,277 scaffolds had a scaffold N50 length of 35.8 Mb and represented an apparent genome size of 1.528 Gb. We used this assembly in combination with Hi-C data generated by Phase Genomics as input for the GAB. The resulting contact maps identified 23 chromosome-sized scaffolds (Fig. 2c), with even the 10 microchromosomes easily delineated from each other (Fig. 2d). Microchromosomes, which are characteristic of avian and reptilian genomes (Waters et al. 2021), pose a particular challenge for Hi-C-based scaffolding due to their small size and the inherently lower signal-to-noise ratios. The GAB method successfully scaffolded these microchromosomes in *A. arizonae* using modularity. This improved the assembly to a final scaffold count of 3,150 and a scaffold N50 length of 106.1 Mb, corresponding to the sixth largest scaffold (Fig. 2e). Similar to the *A. marmoratus* assembly, chromosome-sized scaffolds obtained for *A. arizonae* matched existing karyotype data: one macrochromosome, 12 mid-sized chromosomes, and 10 microchromosomes (Cole et al. 1988; Fig. 2f). Visualization of Hi-C contact maps for each of the 23 chromosomes did not reveal obvious assembly errors (Fig. S5).

The final assemblies of both *A. marmoratus* and *A. arizonae* are contiguous and highly complete, supported by independent metrics. The total scaffold lengths were 1.64 Gb and 1.53 Gb, respectively, with over 99% of each of the sequences anchored within the top 23 scaffolds, corresponding to the haploid chromosome number (Fig. 2g). BUSCO analyses of the genome assemblies further supported high completeness, identifying 97.1% and 95.8%, of conserved single-copy orthologs, respectively (Fig. 2h).

Genome Comparison

Despite both *A. marmoratus* and *A. arizonae* possessing the same karyotype of $2n = 46$, cytogenetic analysis identified specific chromosomal differences that characterize the karyotypes of the *tigris* group, which includes *A. marmoratus*, and the *inornatus* complex that includes *A. arizonae* (Reeder et al. 2002). Our genome-scale comparison supports and extends the findings that the shared chromosome number is the

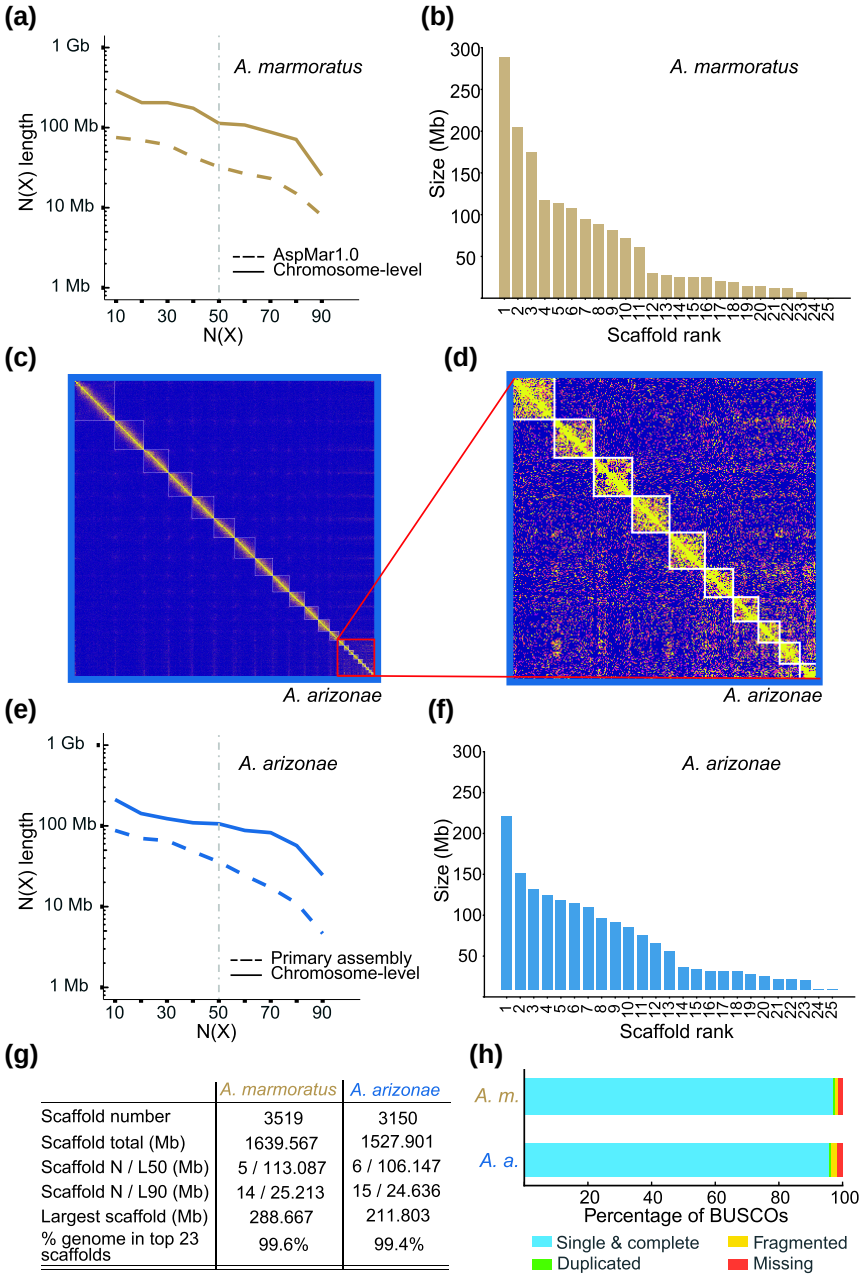

	A. marmoratus	*A. arizonae*
Scaffold number	3519	3150
Scaffold total (Mb)	1639.567	1527.901
Scaffold N / L50 (Mb)	5 / 113.087	6 / 106.147
Scaffold N / L90 (Mb)	14 / 25.213	15 / 24.636
Largest scaffold (Mb)	288.667	211.803
% genome in top 23 scaffolds	99.6%	99.4%

Fig. 2. Genome assembly quality and completeness for *Aspidoscelis marmoratus* and *A. arizonae*. a) N(X) plots comparing the *A. marmoratus* AspMar1.0 assembly (dashed line) and the chromosome-level (solid line) assembly. N(X) indicates the scaffold length such that X% of the total assembly is contained in scaffolds of at least that size. b) Bar plot of the 25 largest scaffolds in the *A. marmoratus* chromosome-level assembly. Over 99% of the assembled genome sequences are assigned to 23 scaffolds. The sizes of the scaffolds are also consistent with the relative sizes of the chromosomes as revealed by karyotype data: three macrochromosomes (>150 Mb), eight mid-sized chromosomes (50 to 150 Mb), and 12 microchromosomes (<50 Mb). c) Order and oriented Hi-C contact maps for the chromosome-level assembly of *A. arizonae*. Contact maps show 23 delineated chromosomes. High contact density along the diagonal indicates strong intrachromosomal interactions, consistent with a well-resolved assembly. d) Zoomed in view of the Hi-C contact maps in c), highlighting the successful grouping and delineation of the 10 microchromosomes in *A. arizonae*. e) N(X) plots comparing the *A. arizonae* primary assembly (dashed line) and the chromosome-level (solid line) assembly. f) Bar plot of the 25 largest scaffolds in the *A. arizonae* chromosome-level assembly. Over 99% of the assembled genome sequences are assigned to 23 scaffolds. The sizes of the scaffolds are also consistent with the relative sizes of the chromosomes as revealed by karyotype data: 1 macrochromosome (>150 Mb), 12 mid-sized chromosomes (50 to 150 Mb), and 10 microchromosomes (<50 Mb). g) Assembly statistics for each species. h) BUSCO completeness scores (queried against vertebrata_odb10, $n = 3354$) for each genome assembly. *A. marmoratus*: single and complete = 97.1%, duplicated: 0.6%, fragmented: 0.9%, missing: 1.4%. *A. arizonae*: single and complete = 95.8%, duplicated = 0.7%, fragmented =1.7%, missing =1.8%.

result of convergent karyotype evolution, as illustrated by a large-scale synteny analysis (Fig. S6).

Based on comparative cytogenetic data presented by Reeder et al. (2002), the predicted *Aspidoscelis* ancestor had $2n = 50$ chromosomes, and the major events that led to the $2n = 46$ karyotype within the *tigris* group are two centric chromosome fusions (Reeder et al. 2002). Our synteny analysis is consistent with this model, revealing that two of the three *A. marmoratus* macrochromosomes are the result of fusion events involving the orthologs of multiple *A. arizonae* chromosomes (Fig. 3a). For example, *A. marmoratus* chromosome 1 is a result of the fusion of *A. arizonae* chromosomes 2 and 3, while *A. marmoratus* chromosome 3 corresponds to the fusion of *A. arizonae* chromosomes 4 and 13. Additionally, the eight mid-sized chromosomes (Set II chromosomes) were previously predicted to harbor pericentric inversions and/or heterochromatin additions. When compared to the corresponding syntenic (otherwise referred to as homeologous) *A. arizonae* chromosome, we observed inversions for seven of the eight chromosome pairs (Fig. 3b). However, we were unable to distinguish between pericentric and paracentric inversions due to the absence of centromere annotations in the current genome assemblies. The apparent "loss" of two microchromosomes in the *inornatus* group can now be explained by fusion events: *A. arizonae* chromosome 1 resulted from a fusion between chromosome 2 and the two smallest microchromosomes (22 and 23) in *A. marmoratus* (Fig. 3a). While a more complex combination of chromosome fission and fusion events cannot be entirely ruled out, the reduction in chromosome number in both species relative to the ancestral karyotype makes the fusions described above the most parsimonious explanation for the observed synteny relationships.

Genome Annotations

Gene prediction across both genomes resulted in highly similar annotations. A total of 29,351 genes (average length = 20,711 bp) were predicted for *A. marmoratus* and 29,572 (average length = 20,427 bp) for *A. arizonae* (Fig. S7A, Table S3). These include both putative protein and nonprotein-coding genes. Functional annotations were assigned based on homology to loci in well-curated databases. Of the predicted genes, 19,387 (*A. marmoratus*) and 19,399 (*A. arizonae*) had at least one functional annotation based on a BLAST search against the UniProt Human Proteome, InterProScan, or EggNOG matches (Fig. 4a and b). BUSCO completeness scores for these transcriptomes were 88.1% for *A. marmoratus* and 87.7% for *A. arizonae*, with less than 1% of duplicated genes for both genomes (Fig. S7A). Gene density was inversely correlated with chromosome size (Fig. 4c and d), a pattern consistent with observations in other reptiles and birds (Waters et al. 2021). We also annotated the mitochondrial genomes of both species, which included the standard vertebrate mitochondrial gene complement of 13 protein-coding genes, 22 tRNAs, and 2 rRNAs (Fig. S7B and C).

Chromosome-by-chromosome analysis of repeat content revealed notable differences in the proportion and composition of repeats among chromosomes in each of the two species (Fig. 4e and f). On average, around 40% of each chromosome was classified as repetitive; however, the distribution of repeat types differed in both species by on the size of the chromosomes. For example, unknown or unclassified repeats are more prevalent on the larger chromosomes, while SINE elements and simple repeats account for a larger fraction of the repeats on the smaller chromosomes. To assess the evolutionary history of repeats in each genome, we examined repeat families (Fig. S8A and B). Both *A. marmoratus* and *A. arizonae* exhibit a prominent peak near a Kimura value of 10, consistent with a major expansion, as well as a smaller shoulder at higher Kimura values (~20), indicating older, more diverged repeat insertions. The lower-divergence peak is enriched with LINEs, DNA transposons such as TcMar and hAT families, and SINEs. Using a range of typical nuclear substitution rates estimated for squamates (~ 2 to 4.5×10^{-9} substitutions/site/year) (Gilbert et al. 2012), this lower-divergence peak corresponds to repeat activity approximately 22 to 50 million years ago. The presence of multiple classified and unclassified repeat families supports the idea that the evolution of these lizard genomes, like other squamates (Pasquesi et al. 2018), is in large part driven by lineage-specific transposable elements and repeat expansion.

Generation of *A. marmoratus* ♀ × *A. arizonae* ♂ Hybrids

A. neomexicanus is a unisexual species that arose from a natural hybridization event (50 to 150 kya) between a female *A. marmoratus* and a male *A. arizonae* (Cole et al. 1988; Barley et al. 2022). Prior attempts at recreating this hybrid failed, but the reciprocal pairing of *A. arizonae* ♀ × *A. marmoratus* ♂ produced viable but sterile progeny (Cole et al. 2010). Here, we report the successful generation of *A. marmoratus* ♀ × *A. arizonae* ♂ F_1 hybrids in the laboratory, mirroring the natural cross that gave rise to *A. neomexicanus*. Hybridization occured when three female *A. marmoratus* were co-housed with a male *A. arizonae* and a male *A. gularis* over a nearly three-year period. During this time, interspecific mating was observed on several occasions, and seven hybrid offspring (four females and three males), from four different clutches, were produced by one of the female *A. marmoratus* and the male *A. arizonae*. These F_1 hybrids were phenotypically similar to *A. neomexicanus*, exhibiting comparable patterning and coloration as hatchlings and adults (Fig. 5a and b). However, unlike *A. neomexicanus*, none of the four hybrid

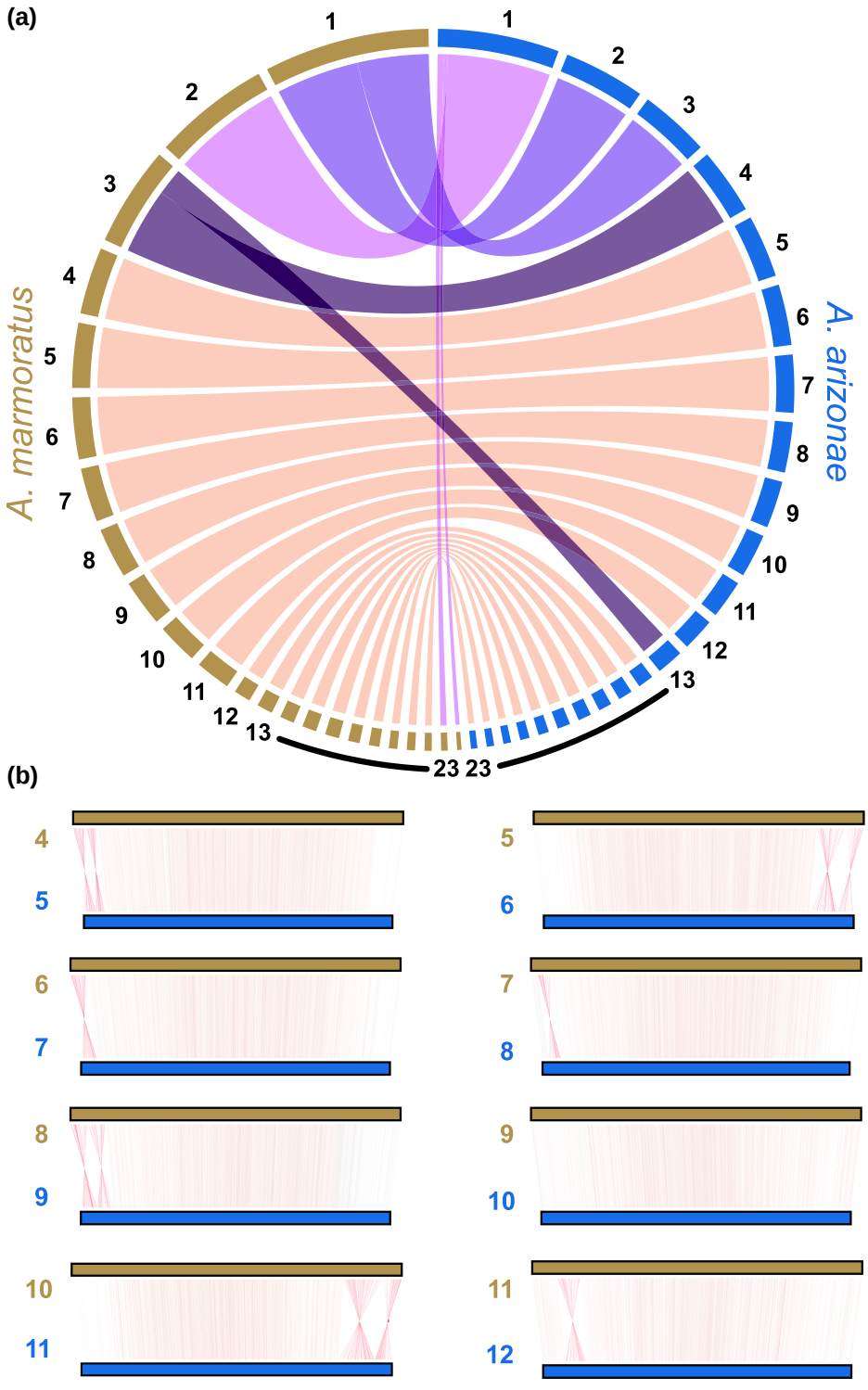

Fig. 3. Comparison between the *Aspidoscelis marmoratus* and *A. arizonae* genomes. a) Circos plot showing the synteny between the 23 *A. marmoratus* and the 23 *A. arizonae* chromosomes. *A. marmoratus* chromosomes are shown in brown (left hemisphere) and *A. arizonae* chromosomes are blue (right hemisphere). Chromosomes are ordered from largest to smallest for each species from the top. Tracks between the chromosomes are colored to indicate 1:1 synteny (tan) or fusions of chromosomes (shades of purple and pink). b) Comparison of *A. marmoratus* Set II chromosomes (as defined in Reeder et al. 2002) with the syntenic chromosomes in *A. arizonae*. Each panels represents a syntenic chromosome pair from the two species, with the chromosome numbers on the left for *A. marmoratus* (brown) and *A. arizonae* (blue). Tan colored lines between the chromosomes show conserved colinearity, while red lines indicate inversions observed within seven of the eight pairs of chromosomes.

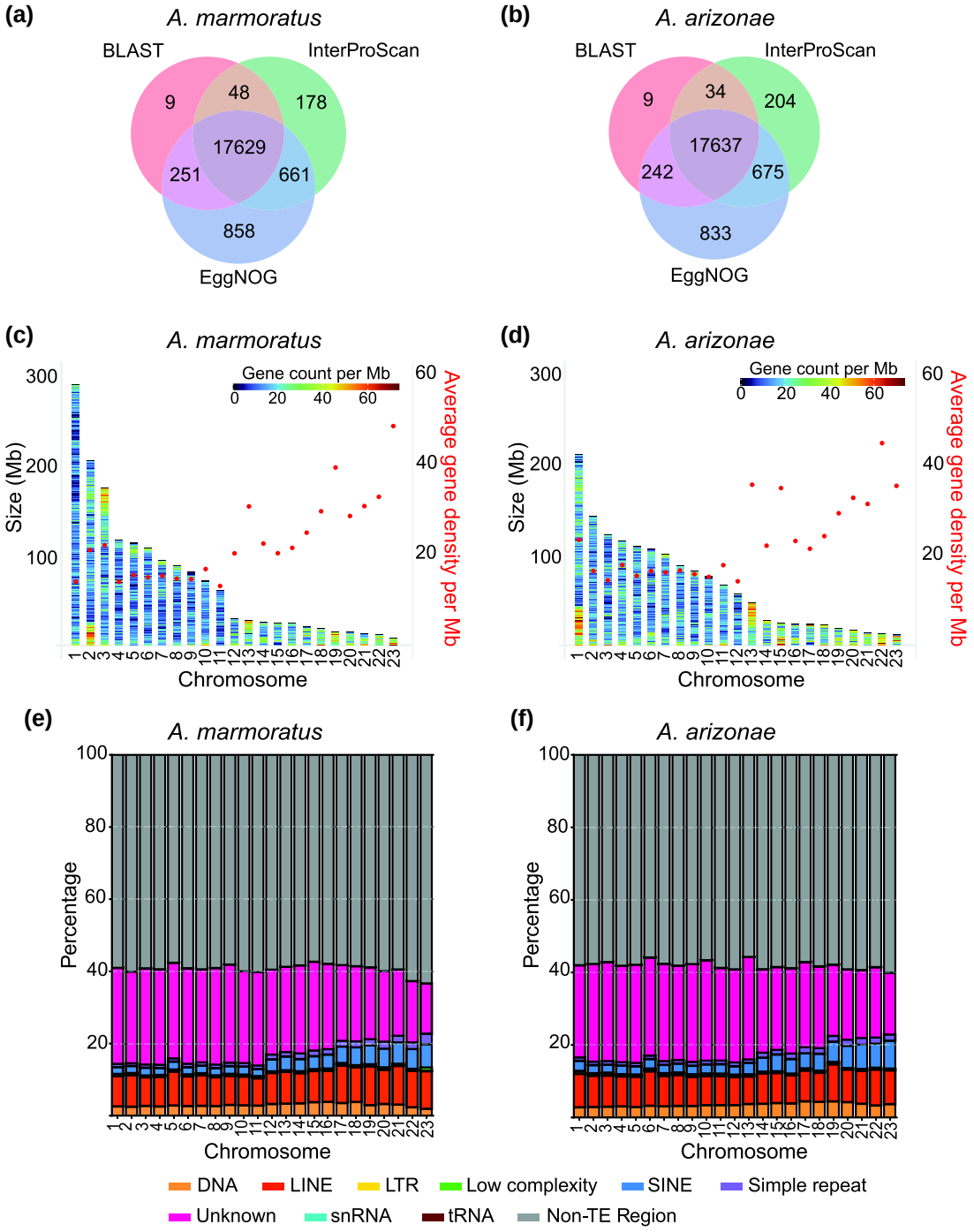

Fig. 4. *Aspidoscelis marmoratus* and *A. arizonae* genome annotations. a) and b) Overlap of functional gene annotations from BLAST search against the UniProt Human Proteome (UP000005640), InterProScan, and EggNOG analyses for *A. marmoratus* and *A. arizonae*, respectively. c) and d) Distribution of functionally annotated genes across the chromosomes for *A. marmoratus* and *A. arizonae*, respectively. The average gene densities (per Mb, ± SD) for each chromosome are in red. e) and f) Prevalence of common repeat element classes on each chromosome for *A. marmoratus* and *A. arizonae*, respectively.

females produced offspring over the course of several years (average = 3.8 years).

Leveraging the newly generated chromosome-level genome assemblies of *A. marmoratus* and *A. arizonae* to investigate genome structure in the hybrids, we performed whole-genome sequencing on four of the F_1 animals. Sequencing reads were mapped to the concatenation of the two parental assemblies, allowing us to assess sequencing coverage across all 46 chromosomes. The resulting profiles revealed even coverage across the entirety of the

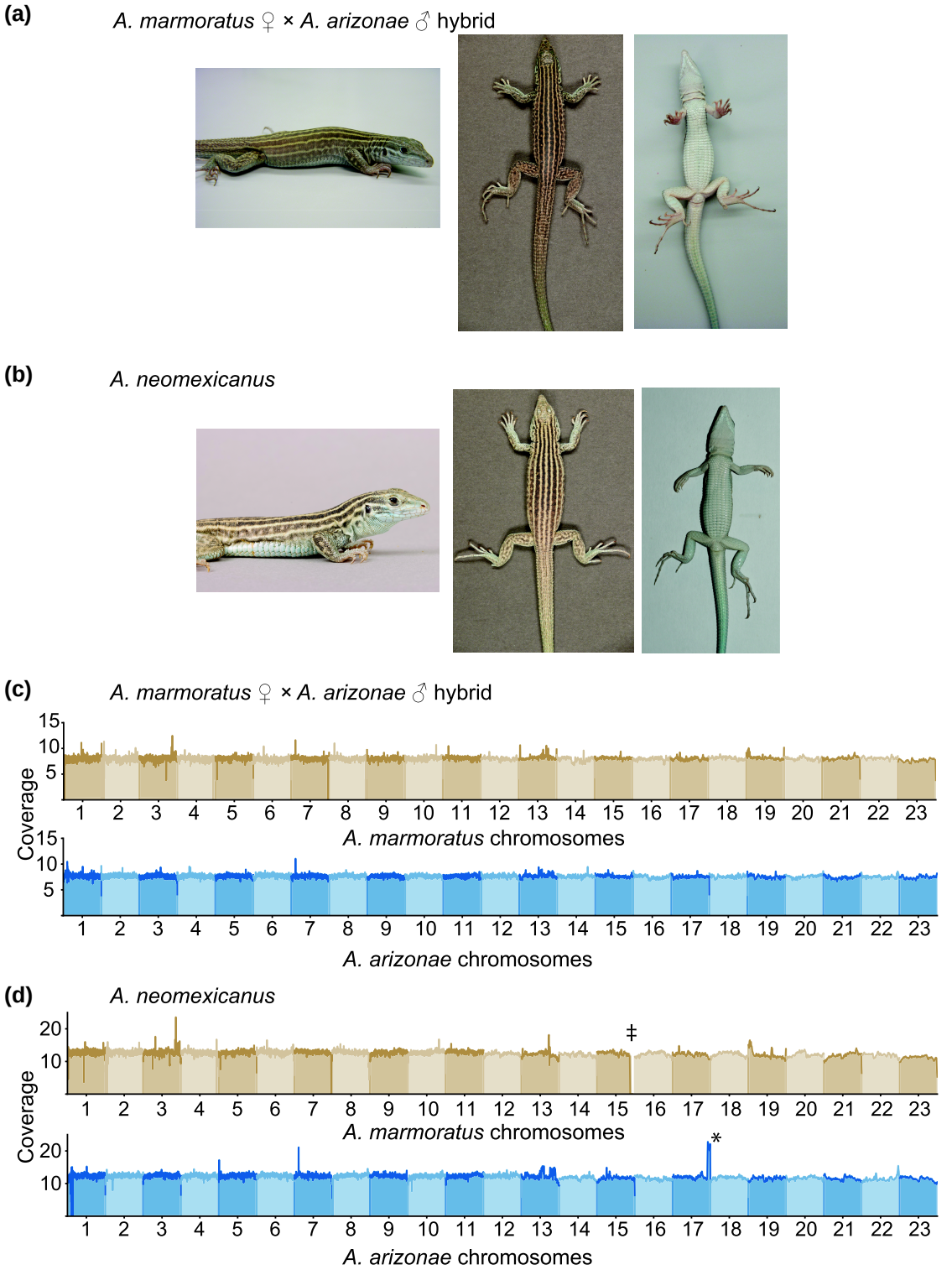

Fig. 5. *Aspidoscelis marmoratus* ♀ × *A. arizonae* ♂ hybrids. a) Pictures of *A. marmoratus* ♀ × *A. arizonae* ♂ hybrid: lateral (left), dorsal (middle), ventral (right). b) Pictures of *A. neomexicanus*: lateral (left), dorsal (middle), ventral (right). c) Coverage plot from whole-genome sequencing of a *A. marmoratus* ♀ × *A. arizonae* ♂ hybrid animal (ID 9642). Reads were mapped to the concatenated *A. marmoratus* and *A. arizonae* reference genomes. Equal sequencing coverage is observed across all 46 chromosomes. d) Coverage plot from whole-genome sequencing of one wild-caught *A. neomexicanus* (ID RLK086). Reads were mapped to the concatenated *A. marmoratus* and *A. arizonae* reference genomes. Equal sequencing coverage is observed across most chromosomes, with a region on *A. marmoratus* chromosome 15 (‡) lacking sequencing coverage and a region on *A. arizonae* chromosome 17 with twice the sequencing coverage (*).

two genomes, consistent with the inheritance of a full haploid set of chromosomes from each parent (Fig. 5c, Fig. S9).

In contrast to the F_1 hybrids, mapping whole-genome sequencing reads from a parthenogenetic *A. neomexicanus* individual to the parental genome assemblies revealed a striking difference on two chromosomes that are syntenic to each other: *A. marmoratus* chromosome 15 and *A. arizonae* chromosome 17 (Fig. 5d). While the sequencing coverage across most of the 46 chromosomes was relatively equal, we observed a complete absence of coverage near the 3′-end of *A. marmoratus* chromosome 15, coupled with an apparent doubling in coverage near the corresponding 3′-end of *A. arizonae* chromosome 17. This pattern indicated that the missing part of *A. marmoratus* chromosome 15 had been replaced by the syntenic *A. arizonae* region on chromosome 17, resulting in LOH. This observation prompted us to conduct a broader investigation into the extent of LOH across multiple *A. neomexicanus* individuals.

Loss of Heterozygosity in *A. neomexicanus*

To characterize patterns of LOH in *A. neomexicanus*, we performed whole-genome sequencing on individuals from both wild and laboratory populations. Two wild-caught individuals were collected from each of three regions in New Mexico: near Albuquerque (Bernalillo County), approximately 11 km north of Socorro (Socorro County), and near Las Cruces (Doña Ana County). Our laboratory colony was derived from five individuals collected approximately 15 km south of Socorro (Fig. 6a). These founder animals had been propagated in captivity for four to eight generations to produce the eight individuals sampled in this study.

We first focused on sequencing coverage across *A. marmoratus* chromosome 15 and *A. arizonae* chromosome 17 (Fig. 6b). In the F_1 hybrids between *A. marmoratus* ♀ and *A. arizonae* ♂ generated in the laboratory, we observed uniform and complete coverage across both chromosomes (Fig. 6b, Fig. S9). In contrast, all *A. neomexicanus* individuals sequenced exhibited LOH near the 3′ ends of this syntenic chromosome pair. Specifically, a loss of coverage on one chromosome was always accompanied by a corresponding twofold increase in coverage on the syntenic region of the other (Fig. 6b, Fig. S10A).

Interestingly, distinct LOH patterns were observed among *A. neomexicanus* individuals regarding *A. marmoratus* chromosome 15 and *A. arizonae* chromosome 17. Each sampling location for the wild animals had its own unique pattern. For the two animals sampled north of Socorro, the coverage profile is consistent with a classical break-induced replication (BIR) event, resulting in LOH for the distal part of the chromosome. Specifically, the terminal region of *A. marmoratus* chromosome 15, starting around 23.24 Mb, is replaced by the terminal portion of *A. arizonae* chromosome 17, starting around 21.27 Mb. While BIR is a common mechanism for LOH near chromosome termini, we cannot rule out the possibility that a crossover followed by inheritance of recombined and nonrecombined chromatids is responsible for the LOH.

Animals from the areas of Albuquerque and Las Cruces exhibit more complex patterns of LOH. For the Albuquerque samples, an internal segment of *A. marmoratus* chromosome 15 (~23.24 to 24.21 Mb) was replaced by the syntenic region from *A. arizonae* chromosome 17 (~21.27 to 22.26 Mb). The Las Cruces individuals display a similar internal LOH pattern and additionally showed a terminal segment of *A. marmoratus* chromosome 15 with twofold coverage, starting around 24.21 Mb, along with a reciprocal loss of the syntenic region from *A. arizonae* chromosome 17. Interestingly, the laboratory animals appeared to exhibit a LOH pattern more similar to the Las Cruces samples, rather than to those from Socorro, despite the founding stock having been collected near Socorro. Closer examination revealed that the breakpoints differ between the laboratory animals and those found in Las Cruces, arguing for separate origins of the respective LOH patterns. In the laboratory animals, a segment of *A. arizonae* chromosome 17 (~21.10 to 22.26 Mb) replaced a region of *A. marmoratus* chromosome 15 (~23.07 to 24.21 Mb), extending the region affected by LOH approximately 170 kb further upstream relative to the break point identified in Albuquerque and Las Cruces animals. Paired-end reads were identified in the alignment files where one mate maps to *A. marmoratus* chromosome 15 and the other to *A. arizonae* chromosome 17, providing direct support for recombination events having occurred within these boundaries. It was not immediately apparent that these genomic regions share unusually high sequence similarity or unusual sequence features.

In addition to evidence for recombination having occurred between *A. marmoratus* chromosome 15 and *A. arizonae* chromosome 17, all eight *A. neomexicanus* individuals from the laboratory colony showed LOH involving *A. marmoratus* chromosome 5 and *A. arizonae* chromosome 6 (Fig. S10B). Four of the eight individuals showed additional LOH involving *A. marmoratus* chromosome 2 and *A. arizonae* chromosome 1 (Fig. S10C). None of these additional sites was observed in any of the wild-caught specimens sequenced here. It is presently not known whether these different patterns were already represented among the founders of our colony or whether the recombination between *A. marmoratus* chromosome 5 and *A. arizonae* chromosome 6 or *A. marmoratus* chromosome 2 and *A. arizonae* chromosome 1 occurred during subsequent generations in captivity. Regardless of the time of origin, the accumulation of LOH events (ranging from ~ 1 Mb to ~10.8 Mb) affects anywhere from 133 to 595 genes

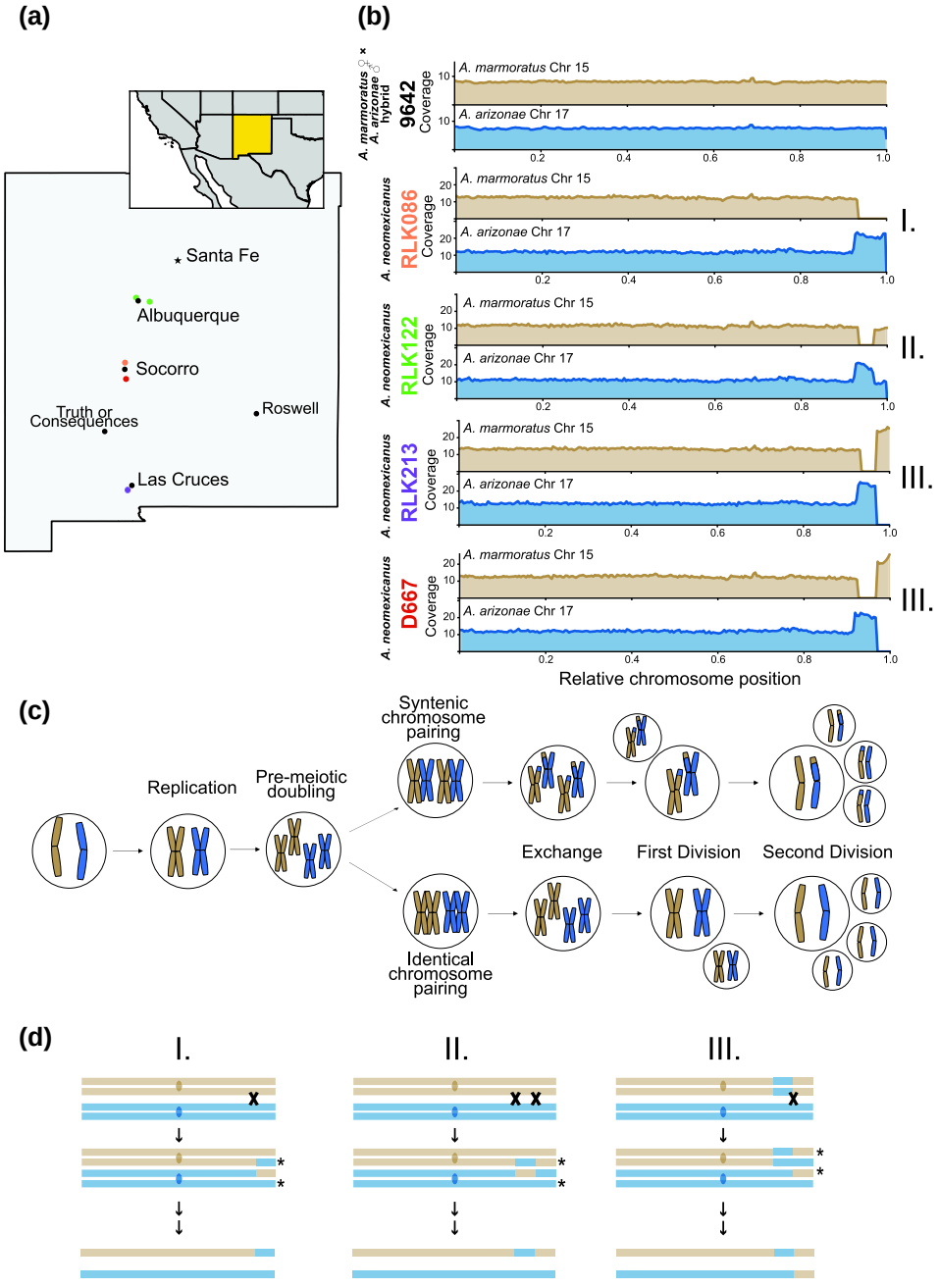

Fig. 6. Loss of heterozygosity in *Aspidoscelis neomexicanus*. a) Map of *A. neomexicanus* sampling localities in New Mexico, USA. There are $n = 2$ for the green dots (near Albuquerque, Bernalillo County), orange dots (north of Socorro, Socorro County), and purple dots (near Las Cruces, Doña Ana County). The red dot indicates the location of where the lab breeding stock was originally collected (south of Socorro). b) Coverage plots for syntenic *A. marmoratus* chromosome 15 and *A. arizonae* chromosome 17 for *A. marmoratus* ♀ × *A. arizonae* ♂ hybrid (ID 9642), three *A. neomexicanus* collected from the wild, each representing one of the sampling locations in (a), and one *A. neomexicanus* from the lab. Color of animal ID corresponds to location in (a). All other sequenced animals are shown in Fig. S10. For the *A. marmoratus* ♀ × *A. arizonae* ♂ hybrid, even and complete coverage was observed across both chromosomes. For all the *A. neomexicanus* samples, even coverage was apparent except for the regions near the 3′ end of the chromosomes where loss of coverage and reciprocal doubling of coverage was observed. In total, three different patterns of LOH were observed and labeled as I., II., III. c) Schematic of meiosis in parthenogenetic whiptail lizards. A single pair of syntenic chromosomes is shown in brown and blue. Following premeiotic replication and an additional doubling in chromosome number, either syntenic chromosomes pair or identical chromosomes pair and recombine. The two meiotic divisions give rise to a diploid oocyte. The majority of pairing occurs between identical chromosomes, leading to the maintenance of heterozygosity in the oocyte, but when syntenic chromosomes pair, loss of heterozygosity may occur. d) Proposed mechanisms of syntenic chromosome pairing of *A. marmoratus* chromosome 15 and *A. arizonae* chromosome 17 during meiosis that leads to the three observed genotypes seen in (b): (I) a single crossover, (II) a double crossover, (III) a single crossover but from an individual already with a genotype similar to type II. * denotes the chromosomes that end up in the developing oocyte.

(Tables S4 to S6) and provides compelling evidence that present day *A. neomexicanus* are a genetically heterogeneous group of lineages.

Discussion

Here, we report chromosome-level genome assemblies for *A. marmoratus* and *A. arizonae*, two highly divergent species within the *Aspidoscelis* clade, whose ancestral hybridization gave rise to the unisexual species *A. neomexicanus*. Even though both species share a $2n = 46$ karyotype, comparative genomics confirmed that identical chromosome numbers are the result of convergence through a pattern of fusion events, rather than being inherited from a common ancestor. We successfully recreated *A. marmoratus* ♀ × *A. arizonae* ♂ hybrids in the laboratory, generating multiple F_1 animals. Unlike *A. neomexicanus*, these F1 hybrids did not reproduce in our facility. Whole-genome sequencing confirmed that they harbor a full complement of chromosomes from each parent. In contrast, whole-genome sequencing of wild-caught and laboratory-propagated *A. neomexicanus* individuals revealed population-specific patterns of LOH affecting several syntenic chromosome pairs. None of the 14 sequenced *A. neomexicanus* animals harbored the full complement of genetic information from both ancestral species. These posthybridization differences in *A. neomexicanus* offer new insights into the maintenance of heterozygosity in unisexuals. While SCP3 staining was consistent with initial pairing occuring either between identical or syntenic chromosomes, fluorescent in situ hybridization supported bivalent formation exclusively between identical chromosomes across dozens of examined oocytes (Lutes et al. 2010; Newton et al. 2016). The discovery of LOH by genomic analysis now indicates that rare pairing and recombination events must occur between syntenic chromosomes.

While mutations have been linked to posthybridization variation between clones (Cole et al. 1988; Taylor et al. 2003), the parental genome assemblies were instrumental in revealing multiple regions of LOH affecting 0.09% to 0.67% of the *A. neomexicanus* genome. This confirms earlier reports of LOH observed in allozyme analysis. For example, gene conversion was hypothesized to explain a homozygous genotype in EST2 in a few individuals of *A. tesselatus*, a diploid unisexual whiptail that arose from the ancestral hybridization of *A. marmoratus* ♀ × *A. scalaris* ♂ (Taylor et al. 2003). Investigation of *A. laredoensis* (diploid unisexual species derived from the ancestral hybridization of *A. gularis* ♀ × *A. sexlineatus* ♂) also identified a few individuals with only one allele for the ESTD locus, while others harbored two distinct alleles (Cole et al. 2020). In light of these prior observations, LOH is likely not restricted to *A. neomexicanus* but affects many or all parthenogenetic species within this genus.

The observation of LOH in *A. neomexicanus* was unexpected considering that premeiotic doubling and identical chromosome pairing ensure the maintenance of genome-wide heterozygosity during oogenesis (Fig. 6c) (Lutes et al. 2010). Furthermore, allozyme analyses (Neaves 1969; Cole et al. 1988, 2010) and skin grafting experiments (Cuellar and McKinney 1976; Cuellar 1977; Persons et al. 2021) had demonstrated that *A. neomexicanus* individuals are highly heterozygous and genetically identical across their range supporting an origin of the species from a single hybridization event. Indeed, the evolutionary success of *A. neomexicanus*, like other unisexual species of hybrid origin, is often attributed to the genome-wide heterozygosity that resulted from interspecific hybridization. The observation of LOH in all *A. neomexicanus* individuals examined in this study, both wild and captive, challenges the idea that only identical chromosomes engage in meiotic pairing, thus maintaining the clonal nature of all individuals within the species. Importantly, since *A. neomexicanus* reproduces by obligate parthenogenesis and not through back-crossing with either parental species, these LOH regions are unlikely to have arisen through introgression. The repeated observation of LOH at syntenic regions on *A. marmoratus* chromosome 15 and *A. arizonae* chromosome 17 suggests that there may be hotspots for the generation of new genotypes. Such pairing, when followed by strand invasion and recombination can result in crossovers and thus LOH in the developing oocyte (Fig. 6d). Alternatively, LOH may be the consequence of BIR involving the homolog as template. Based on the structure of the coverage plots, we infer that the LOH pattern in the wild Socorro samples could have arisen from a single recombination event. In contrast, the Las Cruces samples may reflect two independent successive events. The underlying basis for the prevalence of LOH on specific chromosome pairs remains unresolved, and additional sampling across individuals and populations will be required to determine whether the events are favored by a specific sequence context and whether they are adaptive.

For hybrid unisexual species, the maintenance of heterozygosity is a central theme that bestows them with hybrid vigor. In whiptail lizards, pairing and synapsis between recently duplicated, identical chromosomes circumvents pairing and recombination between the parental genomes. The resulting bivalents pass meiotic checkpoints and the two meiotic divisions generate unreduced oocytes, a process that preserves heterozygosity. Similar mechanisms have been discussed in the context of other unisexual taxa, including loaches (Itono et al. 2006; Juchno et al. 2017), salamanders (Macgregor and Uzzell 1964), geckos (Dedukh et al. 2022), grasshoppers (White et al. 1963), *Darevkia* rock lizards (Dedukh et al. 2024; Spangenberg et al. 2025), and, most recently, the flowerpot snake (*Indotyphlops braminus*) (Lv et al. 2025).

Although the maintenance of heterozygosity is critical for the stability and success of many unisexual lineages, the work presented here adds *A. neomexicanus* to a growing list of examples that suggest LOH is a widespread phenomenon among unisexuals (Tucker et al. 2013; Janko et al. 2021; Jaron et al. 2021). In different systems, LOH has been attributed to varying mechanisms including gene or allelic conversion, as observed in Darevskia rock lizards (Tarkhnishvili et al. 2020) and Bynoe's gecko (*Heteronotia binoei*) (Hillis et al. 1991); intergenomic exchanges between homeologous chromosomes, as in *Ambystoma* salamanders (Bi and Bogart 2006); and automixis, leading to genome-wide LOH in parthenogenetic stick insects (Jaron et al. 2022). Even the ancient asexual bdelloid rotifers exhibit losses of heterozygosity affecting up to 4.5 Mb of their genome (Simion et al. 2021). Similar to the variable patterns of LOH across different *A. neomexicanus* populations, a recent study reported variable LOH in the flowerpot snakes from different parts of Asia (Lv et al. 2025). Together, these examples highlight that the gradual erosion of heterozygosity is an inherent risk of unisexuality that may well play a critical role in limiting the evolutionary lifespan of the species. However, depending on the frequency, extent, and targets of LOH, some unisexual lineages may persist by tolerating losses at loci that are selectively neutral or deleterious, or conversely, LOH could be advantageous for some loci under specific conditions. Our results underscore the broader value of high-quality reference genomes, not only for understanding the structure and history of sexual species, but also for monitoring genomic instability in unisexual lineages of hybrid origin.

Beyond the present study, chromosome-level assemblies for *A. marmoratus* and *A. arizonae* will be a valuable genomic resource for studying squamate biology and offer new opportunities for investigating the genomic consequences of hybridization. While sequencing efforts across reptiles have increased in recent years, high-quality chromosome-scale assemblies remain relatively rare. As of April 2025, there were only 292 reference genomes available for squamates in GenBank, and only 65 of them were at chromosome-level (last access April 30, 2025) (Clark et al. 2016). As the total number of described squamate species continue to rise, with an average of over 200 new species added each year (Uetz et al. 2025), more high-quality genome assemblies will be valuable for comparative genomics (Smith et al. 2020; Gable et al. 2023) and to capitalize on the many opportunities presented by squamates as model systems in areas such as regeneration and aging. Furthermore, squamates represent diverse modes of reproduction (Sites et al. 2011), sex determination (Pokorná and Kratochvíl 2009), and genome size and organization (Waters et al. 2021), all areas in which reference genomes are necessary to begin to understand the genomic and molecular basis and evolutionary processes.

Materials and Methods

Animals

Laboratory animals used in this study were produced in the AAALAC International accredited Stowers Reptile and Aquatics Facility at the Stowers Institute for Medical Research (SIMR) under protocols approved by the Institutional Animal Care and Use Committee (IACUC number 2015-1040), and at Johannes Gutenberg University (JGU) in accordance with all relevant ethical regulations for animal use as approved by the Veterinary Office (Landesuntersuchungsamt) of Rheinland-Palatinate, Germany. All study animals descended from breeding stock collected in New Mexico under permit numbers 3199 and 3395.

Some field-collected animals used in this study were captured using a snare pole under scientific collections permits authorized by the New Mexico Department of Game and Fish (number 3670) and the State Parks Division of the Energy, Minerals and Natural Resources Department. The use of these animals for scientific purposes was approved by the Auburn University IACUC (2018-3286).

Genome Assembly and Statistics

For the *A. marmoratus* assembly, liver tissue from the same animal (ID 8450) used for the AspMar1.0 assembly (GCA_014337955.1) was used for Hi-C library preparation. Two libraries were created at Dovetail Genomics, sequenced at the SIMR Molecular Biology Core Facility on an Illumina HiSeq 2500 (2 × 100 bp), and subjected to the Dovetail Genomics HiRise genome assembly algorithm with the AspMar1.0 assembly to produce a chromosome-level assembly.

For the initial *A. arizonae* assembly, liver from a wild-caught animal (ID 17121) collected near Alamogordo, New Mexico, USA (32°52′55″ N, 105°57′47″ W) was used to generate short-read Illumina libraries (2 × 250 bp) at SIMR (KAPA HTP Library Prep Kit; KK8234) and Chicago libraries at Dovetail Genomics (2 × 100 bp). The libraries were sequenced on an Illumina HiSeq2500 at SIMR. K-mer frequency distributions were generated from the trimmed short-read data using KMC (v. 3.1.0) (Kokot et al. 2017) with a k-mer size of 21, and genome size was subsequently estimated with GenomeScope2 (Ranallo-Benavidez et al. 2020). Trimming was performed with Trimmomatic (v. 0.36) (Bolger et al. 2014) using the following parameters: `PE -phred 33 LEADING:3 TRAILING:3 SLIDING WINDOW:4:15 MINLEN:36`. The following parameters were used for KMC: `-k21 -m64 -ci1 -cs10000`. Both short-read and Chicago libraries were used to produce a primary assembly with HiRise by Dovetail Genomics. Hi-C library construction and sequencing were performed at Phase Genomics (Seattle, Washington, USA). Using the

primary assembly and the Hi-C data, a chromosome-level assembly for *A. arizonae* was completed through scaffolding using the GAB.

In brief, the Hi-C data is aligned to the primary assembly using Hi-C Pro to produce normalized genome-wide contact maps (Servant et al. 2015). Afterwards, the contact maps are used to cluster genomic loci based solely on contact frequencies using the unweighted pair group method with arithmetic mean (UPGMA) clustering to infer chromosome groups, without requiring prior scaffolding information (Fig. S1B). This enables unbiased and dynamic separation of chromosomes regardless of their size, a property that is particularly important for species with highly variable chromosome sizes.

Initial chromosome groupings are identified using either a Hidden Markov Model or a hypergeometric test algorithm, and smaller loci are assigned using the modularity Louvain method for community detection (Blondel et al. 2008). This concept, originally developed in network theory, has been adopted in evolutionary biology to help identify and explain gene networks and compartmentalizing complex systems into distinct parts (Melo et al. 2016; Hatleberg and Hinman 2021). Here, we adapted it to genome scaffolding by treating loci as nodes and Hi-C contact frequencies as edges, allowing the algorithm to identify densely interacting chromosomal regions. Scaffolds were ordered and oriented via a two-phase permutation search strategy that prioritizes larger scaffolds with stronger contact signals, followed by iterative refinement. Together, these strategies allow GAB to efficiently and accurately organize genome sequences into chromosomes (more details available in Supplementary methods).

For implementation, GAB requires output from HiC-Pro pipeline (v. 2.11.1) (Servant et al. 2015) and uses its output as input for scaffolding. The Hi-C data were first trimmed with trimmomatic (v. 0.36; `LEADING:3 TRAILING:3 SLIDINGWINDOW:4:15 MINLENGTH:50`). The primary assembly was run through HiC-Pro's digest genome script (digest_genome.py) to identify the restriction fragments in the primary assembly with GATC as the restriction site for this specific Hi-C library. Parameters important in the HiC-Pro configuration file are as follows: `BOWTIE2_GLOBAL_OPTIONS = –very-sensitive -L 30 –score-min L, –0.6, –0.2 –end-to-end –reorder, BOWTIE2_LOCAL_OPTIONS = –very-sensitive-L 20 –score-min L, –0.6, –0.2 –end-to-end –reorder, LIGATION_SITE = GATCGATC, GET_ALL_INTERACTION_CLASSES = 1, GET_PROCESS_SAM = 0, RM_SINGLETON = 0, RM_MULTI = 0, RM_DUP = 1, MAX_ITER = 125, FILTER_LOW_COUNT_PERC = 0.02, FILTER_HIGH_COUNT_PERC = .01, EPS = 0.1.`

In order to assess the completeness of the *A. marmoratus* and *A. arizonae* assemblies, we used BUSCO (v. 5.4.2) (Simão et al. 2015) in genome mode with the vertebrate_od10 dataset. To assess the accuracy of the genome assembly, valid Hi-C read pairs mapping within the same chromosome were used for detailed visualization. For each chromosome, the relative positions of read pairs were plotted. The resulting scatterplots allow the identification of potential assembly errors by visualizing the spatial distribution and orientation of read pairs. In a correctly assembled scaffold, read pairs are expected to cluster tightly along the x-axis. Satsuma (v. 2.0) (Grabherr et al. 2010) under default settings was used to perform whole genome synteny analysis between the 23 chromosomes of the *A. marmoratus* (as the target) and *A. arizonae* (as the query) chromosome-level assemblies. Synteny dotplots and collinearity plots were generated from the Satsuma output.

Single-Chromosome Isolation, Sequencing, and Analysis

Chromosome spreads were prepared from embryonic fibroblast cell cultures of *A. marmoratus*. Cells were harvested by trypsin treatment and treated with 75 mM KCl for 5 min at room temperature, then fixed with methanol:acetic acid (3:1). Fixed cell suspension was dropped on a membrane slide (Zeiss, Germany) and allowed to dry at room temperature. Chromosome spreads on membrane slides were stained Giemsa's stain solution (EMD Millipore, USA), and the three largest chromosomes were identified as chromosomes 1, 2, and 3, by their respective sizes. The chromosomes were captured and collected each in adhesive caps (Zeiss, Germany) on a laser capture microdissection with PALM microbeam system (Zeiss, Germany). Collected chromosomes on adhesive caps were suspended in 5 µL of cell extraction buffer, then centrifuged. Lysis and amplification of chromosomal DNA were performed according to the manufacturer's instruction (PicoPLEX DNA-seq Kit #R300381; Rubicon Genomics, USA). For preamplification and amplification, 14 and 9 cycles were used, respectively. Each of the amplified samples was cleaned up using 1× AMPure XP beads. In total, four successful libraries were made and sequenced (1 × 100 bp) on RapidSeq flow cells with an Illumina HiSeq 2500 at SIMR: a single isolated chromosome 1, a pool of 12 copies of chromosome 1, a pool of 9 copies of chromosome 2, and a pool of 11 copies of chromosome 3.

Adapter sequences and the first 14 bases were removed from all reads with Trimmomatic (v. 0.36) with the following parameters: `SE HEADCROP:14 LEADING:3 TRAILING:3 SLIDINGWINDOW:4:15 MINLENGTH:35`. The reads were aligned with bwa mem (v. 0.7.17) (Li and Durbin 2010) to the concatenation of the newly generated *A. marmoratus* chromosome-level assembly + human reference genome (hg38) + UniVec database (Suryamohan et al. 2020). Human and UniVec sequences were included to filter out potential contamination. PCR duplicates were

marked with PicardTools (v. 2.6.0) (https://broadinstitute.github.io/picard/) and only reads with a mapping quality of 60 were retained. BigWig tracks were generated from the alignment files with deepTools/bamCoverage (v. 3.5.2) (Ramírez et al. 2016) with the following parameters: `–binSize 50 –normalizeUsing CPM`. The tracks were visualized with karyoploteR (v. 1.22.0) (Gel and Serra 2017) by rendering the bigWig over the corresponding chromosome, and the *y*-axis represents the counts per million (CPM) per 50 bp.

Gene and Repeat Content Annotation

Total RNA derived from various tissues (whole body, testes, brains, thigh muscle, heart, lung, liver, follicles, and germinal beds) was extracted using TRIzol, treated with DNase, and cleaned up using the QIAGEN RNeasy Mini Kit (Table S1). Paired-end RNA sequencing was performed on RNA samples that had been either ribosomal RNA–depleted or poly(A)-selected. To maximize transcript discovery, we generated both poly(A)-selected and rRNA-depleted RNA-seq libraries because these enrich distinct RNA classes. The sequencing data were used to generate intronic hint files for annotations. Gene annotations for *A. marmoratus* and *A. arizonae* assemblies were established simultaneously using Augustus-Comparative Gene Prediction (CGP; v. 3.4.0) (Nachtweide and Stanke 2019) due to the high relation between species. Whole genome alignment using minimap2 (v. 2.17) (Li 2018) was completed using the following parameters to ensure large alignment segments: `-B 1 -A 50 -O 3,3 -E 1,1 –cs=long`. Briefly, RNA-sequencing data were trimmed using trimmomatic (v. 0.36) (parameters: `SLIDINGWINDOW:5:20 LEADING:10 TRAILING:10 MINLEN:70`) and aligned to their respective assemblies using STAR (v. 2.7.8a) (Dobin et al. 2013). The resulting alignment was processed by samtools (v. 1.12) (Danecek et al. 2021) and converted into a hints file by Augustus' bam2hints script. Augustus CGP was run with the whole-genome alignment, the generated hint files, and a uniform star-based phylogenetic tree with no outgroup as input. Overlapping gene predictions were collapsed into single transcript predictions using GFFCompare (v. 0.12.6) (Pertea and Pertea 2020) and custom scripts. Protein sequences were created from the resulting annotations using GffRead (v. 0.12.7) (Pertea and Pertea 2020) and translated by transeq from EMBOSS (v. 6.6.0.0) (Rice et al. 2000). Functional annotation was completed using BLAST (v. 2.11.0) (Camacho et al. 2009) search against the UniProt Human Proteome (UP000005640), EggNOG (v. 2.1.6) (Cantalapiedra et al. 2021), and InterProScan (v. 5.52-86.0) (Jones et al. 2014). Annotated genes within 80 kb of each other that had a BLAST to the same reference protein were combined. Overlapping annotations were again collapsed into single transcript predictions as previously described. We note that our annotation pipeline of merging of overlapping predictions may occasionally collapse nearby paralogs, which could affect detailed gene family analyses. Single exon genes not BLASTing against SinEx DB 2.0 with a percent identity of at least 70% across at least 60% of the database gene were removed. Annotation completeness was measured using BUSCO (v. 5.0.0) in transcriptome mode with the vertebrata_odb10 database.

To quantify and assess the repetitive content, we used the RepeatMasker (v. 4.0.9) (Smit et al. 2008) pipeline. We first generated a de novo list of repeat elements using RepeatModeler (v. 1.0.11) (Smit and Hubley 2008) and used this as input for RepeatMasker using the NCBI/RMBLAST (v. 2.6.0+) search engine.

Both mitochondrial genomes were assembled de novo using NOVOPlasty (v. 4.3.3) (Dierckxsens et al. 2017) with the short-read data generated here for *A. arizonae* and the previously uploaded short-read data for *A. marmoratus* (ID 8450; BioProject PRJNA360150). The COX1 sequence from *A. inornatus* (NCBI Accession NC_067819) was used as the seed sequence with a k-mer parameter set to 65. Gene annotations of the mitochondrial genomes were performed in Geneious guided by the *A. inornatus* mitochondrial genome (NCBI Accession NC_067819).

Sequencing and Analysis of *A. marmoratus* ♀ × *A. arizonae* ♂ Hybrids and *A. neomexicanus*

The *A. marmoratus* ♀ × *A. arizonae* ♂ hybrids were all offspring from the same *A. marmoratus* (ID 122) and the same *A. arizonae* (ID 4272). Founder animals representing *A. m. marmoratus* and *A. a. llanuras*, collected near Hot Springs (Sierra County) and Alamogordo (Otero County), New Mexico, USA, respectively, gave rise to the two parental individuals (ID 122 and ID 4272).

Genomic DNA from the *A. marmoratus* ♀ × *A. arizonae* ♂ hybrids and *A. neomexicanus* were extracted from either tail or liver tissue using the QIAGEN Genomic-tip 100/G (cat. no. 10243) protocol and subsequently fragmented with a Covaris Sonicator (Table S2). Library preparation for whole-genome sequencing was performed using either KAPA HTP Library Prep Kit or NEBNext Ultra II DNA Library Prep Kit. The libraries were sequenced with on a HiSeq 2500 or NextSeq 2000.

Trimmomatic (v. 0.36; `PE -phred 33 LEADING:3 TRAILING:3 SLIDINGWINDOW:4:15 MINLEN:36`) was used to remove adapters and was aligned to the concatenated *A. marmoratus* and *A. arizonae* genome assemblies using bwa (v. 0.7.17). Sequencing coverage plots were generated from values calculated across the 46 chromosomes using pysam (v. 0.12.0.1; https://github.com/pysam-developers/pysam) on the alignment files. We only considered reads with a mapping quality of 60 and

excluded supplementary alignments (i.e. reads that are split across multiple locations with the 0 × 800 flag). Per-base coverage was aggregated in nonoverlapping 100 kb bins. To account for repetitive and low-complexity regions, masked intervals were derived from the previous RepeatMasker annotations, and bases overlapping these masked intervals were excluded from coverage calculations. Bins in which fewer than 25% of bases remained unmasked were assigned a coverage value of zero. Additionally, positions with pileup depth exceeding 100 were ignored to mitigate the effects of PCR duplicates or collapsed repeats. Regions of LOH were identified by visually inspecting the normalized coverage plots for reciprocal changes in coverage between syntenic chromosome pairs.

Supplementary Material

Supplementary material is available at *Genome Biology and Evolution* online.

Acknowledgments

We mourn with deep sadness the loss of our coauthor and friend William B. Neaves, who passed away while this manuscript was under review. His curiosity, integrity, and warmth enriched both our research and all who worked with him. We are grateful for his contributions and cherish his memory.

We are grateful for the husbandry staff at the SIMR especially Rick Kupronis and the team of dedicated reptile technicians (David Jewell, Alex Muensch, Jillian Schieszer, Christina Piraquive, and Kristy Winter) for outstanding husbandry and herpetocultural skills. We also thank Martin Fahr and his colleagues for animal husbandry at JGU. Field collections were made possible with the help of C. Painter, L. Miles Horne, Tori Herron, Ryan Cook, Océane Da Cunha, José Maldonado, and Gary Gruer. Assistance with RNA extractions was provided by Rachel Helston, and Lisa Lassise at SIMR facilitated coordination and communication with commercial entities. We thank Konstantin L. Wittkopp for providing professional photographic services used in this manuscript. Sequencing support came from the Molecular Biology Core Facility at SIMR, the Nucleic Acid Core Facility at JGU, and the Genomics Core Facility at the IMB. We further acknowledge computing time granted on the supercomputer MOGON II at JGU as part of NHR South-West (nhrsw.de), as well as the IMB Bioinformatics Core and the Institute for Quantitative and Computational Biosciences for computing resources and support. This work was funded in part by the Howard Hughes Medical Institute, SIMR, and an Alexander von Humboldt Professorship awarded to P.B. at JGU. Additionally, this project was funded in part by the Deutsche Forschungsgemeinschaft (DFG, German Research Foundation) – GRK2526 – Project no. 407023052.

Data Availability

All raw sequencing data pertaining to the *A. marmoratus* (PRJNA360150, AspMarm2.0) and *A. arizonae* (PRJNA1260700, AspAri2.0) genome assemblies are available at the National Center for Biotechnology Information under project accession number PRJNA1260518 and PRJNA1260700, respectively. All other sequencing data can be found under the following project accession numbers: PRJNA1260499 (single-chromosome sequencing), PRJNA1260429 (RNA-sequencing), and PRJNA1259779 (whole-genome sequencing). Code for analysis is available at https://github.com/baumannlab/Aspi_Genomes. The Genome Assembly Booster is available at https://github.com/baumannlab/Genome_Assembly_Booster.

Literature Cited

Barley AJ, et al. Complex patterns of hybridization and introgression across evolutionary timescales in Mexican whiptail lizards (*Aspidoscelis*). Mol Phylogenet Evol. 2019:132:284–295. https://doi.org/10.1016/j.ympev.2018.12.016.

Barley AJ, Nieto-Montes de Oca A, Manríquez-Morán NL, Thomson RC. The evolutionary network of whiptail lizards reveals predictable outcomes of hybridization. Science. 2022:377:773–777. https://doi.org/10.1126/science.abn1593.

Bi K, Bogart JP. Identification of intergenomic recombinations in unisexual salamanders of the genus *Ambystoma* by genomic in situ hybridization (GISH). Cytogenet Genome Res. 2006:112:307–312. https://doi.org/10.1159/000089885.

Blondel VD, Guillaume J-L, Lambiotte R, Lefebvre E. Fast unfolding of communities in large networks. J Stat Mech. 2008:2008:P10008. https://doi.org/10.1088/1742-5468/2008/10/P10008.

Bolger AM, Lohse M, Usadel B. Trimmomatic: a flexible trimmer for Illumina sequence data. Bioinformatics. 2014:30:2114–2120. https://doi.org/10.1093/bioinformatics/btu170.

Camacho C, et al. BLAST+: architecture and applications. BMC Bioinform. 2009:10:421. https://doi.org/10.1186/1471-2105-10-421.

Cantalapiedra CP, Hernández-Plaza A, Letunic I, Bork P, Huerta-Cepas J. eggNOG-mapper v2: functional annotation, orthology assignments, and domain prediction at the metagenomic scale. Mol Biol Evol. 2021:38:5825–5829. https://doi.org/10.1093/molbev/msab293.

Clark K, Karsch-Mizrachi I, Lipman DJ, Ostell J, Sayers EW. GenBank. Nucleic Acids Res. 2016:44:D67–D72. https://doi.org/10.1093/nar/gkv1276.

Cole CJ, et al. The second known tetraploid species of parthenogenetic tetrapod (Reptilia: Squamata: Teiidae): description, reproduction, comparisons with ancestral taxa, and origins of multiple clones. Bull Mus Comp Zool. 2017:161:285–321. https://doi.org/10.3099/MCZ37.1.

Cole CJ, et al. Reticulate phylogeny: a new tetraploid parthenogenetic whiptail lizard derived from hybridization among four bisexual ancestral species of *Aspidoscelis* (Reptilia: Squamata: Teiidae). Bull Mus Comp Zool. 2023:163:247–279. https://doi.org/10.3099/MCZ76.

Cole CJ, Dessauer HC, Barrowclough GF. Hybrid origin of a unisexual species of whiptail lizard, Cnemidophorus neomexicanus, in western North America: new evidence and a review. American Museum of Natural History; 1988. https://www.biodiversitylibrary.org/item/317104.

Cole CJ, Dessauer HC, Paulissen MA, Walker JM. Hybridization between whiptail lizards in Texas: Aspidoscelis laredoensis and *A. gularis*, with notes on reproduction of a hybrid. Am Mus Novit. 2020:2020:1–13. https://doi.org/10.1206/3947.1.

Cole CJ, Hardy LM, Dessauer HC, Taylor HL, Townsend CR. Laboratory hybridization among North American whiptail lizards, including Aspidoscelis inornata arizonae x A. tigris marmorata (Squamata, Teiidae), ancestors of unisexual clones in nature. American Museum of Natural History; 2010. https://www.biodiversitylibrary.org/item/280199

Cole CJ, Taylor HL, Baumann DP, Baumann P. Neaves' whiptail lizard: the first known tetraploid parthenogenetic tetrapod (Reptilia: Squamata: Teiidae). Breviora. 2014:539:1–20. https://doi.org/10.3099/MCZ17.1.

Cuellar O. Genetic homogeneity and speciation in the parthenogenetic lizards *Cnemidophorus velox* and *C. neomexicanus*: evidence from intraspecific histocompatibility. Evolution. 1977:31:24–31. https://doi.org/10.1111/j.1558-5646.1977.tb00978.x.

Cuellar O, McKinney CO. Natural hybridization between parthenogenetic and bisexual lizards: detection of uniparental source by skin grafting. J Exp Zool. 1976:196:341–350. https://doi.org/10.1002/jez.1401960308.

Danecek P, et al. Twelve years of SAMtools and BCFtools. GigaScience. 2021:10:giab008. https://doi.org/10.1093/gigascience/giab008.

Dedukh D, et al. Premeiotic endoreplication is the mechanism of obligate parthenogenesis in rock lizards of the genus Darevskia. Biol Lett. 2024:20:20240182. https://doi.org/10.1098/rsbl.2024.0182.

Dedukh D, Altmanová M, Klíma J, Kratochvíl L. Premeiotic endoreplication is essential for obligate parthenogenesis in geckos. Development. 2022:149:dev200345. https://doi.org/10.1242/dev.200345.

Dierckxsens N, Mardulyn P, Smits G. NOVOPlasty: de novo assembly of organelle genomes from whole genome data. Nucleic Acids Res. 2017:45:e18. https://doi.org/10.1093/nar/gkw955.

Dobin A, et al. STAR: ultrafast universal RNA-seq aligner. Bioinformatics. 2013:29:15–21. https://doi.org/10.1093/bioinformatics/bts635.

Gable SM, et al. The state of squamate genomics: past, present, and future of genome research in the most speciose terrestrial vertebrate order. Genes (Basel). 2023:14:1387. https://doi.org/10.3390/genes14071387.

Gel B, Serra E. Karyoploter: an R/Bioconductor package to plot customizable genomes displaying arbitrary data. Bioinformatics. 2017:33:3088–3090. https://doi.org/10.1093/bioinformatics/btx346.

Gilbert C, Hernandez SS, Flores-Benabib J, Smith EN, Feschotte C. Rampant horizontal transfer of SPIN transposons in squamate reptiles. Mol Biol Evol. 2012:29:503–515. https://doi.org/10.1093/molbev/msr181.

Grabherr MG, et al. Genome-wide synteny through highly sensitive sequence alignment: satsuma. Bioinformatics. 2010:26:1145–1151. https://doi.org/10.1093/bioinformatics/btq102.

Hatleberg WL, Hinman VF. Chapter two—modularity and hierarchy in biological systems: using gene regulatory networks to understand evolutionary change. In: Gilbert SF, editors. Current topics in developmental biology. Evolutionary developmental biology. Vol. 141. Academic Press; 2021. p. 39–73. https://doi.org/10.1016/bs.ctdb.2020.11.004.

Hillis DM, Moritz C, Porter CA, Baker RJ. Evidence for biased gene conversion in concerted evolution of ribosomal DNA. Science. 1991:251:308–310. https://doi.org/10.1126/science.1987647.

Ho DV, et al. Post-meiotic mechanism of facultative parthenogenesis in gonochoristic whiptail lizard species. eLife. 2024:13:e97035. https://doi.org/10.7554/eLife.97035.

Hotaling S, Kelley JL, Frandsen PB. Toward a genome sequence for every animal: where are we now? Proc Natl Acad Sci. 2021:118:e2109019118. https://doi.org/10.1073/pnas.2109019118.

Uetz P, et al. 2025. The Reptile Database. http://www.reptile-database.org

Itono M, et al. Premeiotic endomitosis produces diploid eggs in the natural clone loach, misgurnus anguillicaudatus (Teleostei: Cobitidae). J Exp Zool A Comp Exp Biol. 2006:305A:513–523. https://doi.org/10.1002/jez.a.283.

Janko K, et al. Genome fractionation and loss of heterozygosity in hybrids and polyploids: mechanisms, consequences for selection, and link to gene function. Mol Biol Evol. 2021:38:5255–5274. https://doi.org/10.1093/molbev/msab249.

Jaron KS, et al. Genomic features of parthenogenetic animals. J Hered. 2021:112:19–33. https://doi.org/10.1093/jhered/esaa031.

Jaron KS, et al. Convergent consequences of parthenogenesis on stick insect genomes. Sci Adv. 2022:8:eabg3842. https://doi.org/10.1126/sciadv.abg3842.

Jones P, et al. InterProScan 5: genome-scale protein function classification. Bioinformatics. 2014:30:1236–1240. https://doi.org/10.1093/bioinformatics/btu031.

Juchno D, Arai K, Boroń A, Kujawa R. Meiotic chromosome configurations in oocytes of cobitis taenia and its polyploid hybrids. Ichthyol Res. 2017:64:240–243. https://doi.org/10.1007/s10228-016-0556-1.

Kokot M, Długosz M, Deorowicz S. KMC 3: counting and manipulating k-mer statistics. Bioinformatics. 2017:33:2759–2761. https://doi.org/10.1093/bioinformatics/btx304.

Li H. Minimap2: pairwise alignment for nucleotide sequences. Bioinformatics. 2018:34:3094–3100. https://doi.org/10.1093/bioinformatics/bty191.

Li H, Durbin R. Fast and accurate long-read alignment with Burrows-Wheeler Transform. Bioinformatics. 2010:26:589–595. https://doi.org/10.1093/bioinformatics/btp698.

Lowe CH, Wright JW. Evolution of parthenogenetic species of Cnemidophorus (whiptail lizards) in western North America. J Ariz Acad Sci. 1966:4:81–87.

Lutes A, Baumann D, Neaves W, Baumann P. Laboratory synthesis of an independently reproducing vertebrate species. Proc Natl Acad Sci USA. 2011:108:9910–9915. https://doi.org/10.1073/pnas.1102811108.

Lutes AA, Neaves WB, Baumann DP, Wiegraebe W, Baumann P. Sister chromosome pairing maintains heterozygosity in parthenogenetic lizards. Nature. 2010:464:283–286. https://doi.org/10.1038/nature08818.

Lv Y, et al. Genomic insights into evolution of parthenogenesis and triploidy in the flowerpot snake. Sci Adv. 2025:11:eadt6477. https://doi.org/10.1126/sciadv.adt6477.

Macgregor HC, Uzzell TM. Gynogenesis in salamanders related to *Ambystoma jeffersonianum*. Science. 1964:143:1043–1045. https://doi.org/10.1126/science.143.3610.1043.

Melo D, Porto A, Cheverud JM, Marroig G. Modularity: genes, development and evolution. Annu Rev Ecol Evol Syst. 2016:47:463–486. https://doi.org/10.1146/annurev-ecolsys-121415-032409.

Nachtweide S, Stanke M. Multi-genome annotation with AUGUSTUS. Methods Mol Biol. 2019:1962:139–160. https://doi.org/10.1007/978-1-4939-9173-0_8.

Neaves WB. Adenosine deaminase phenotypes among sexual and parthenogenetic lizards in the genus *Cnemidophorus* (Teiidae). J Exp Zool. 1969:171:175–183. https://doi.org/10.1002/jez.1401710205.

Neaves WB. Tetraploidy in a hybrid lizard of the genus *Cnemidophorus* (Teiidae). Breviora. 1971:381:1–25.

Newton AA, et al. Widespread failure to complete meiosis does not impair fecundity in parthenogenetic whiptail lizards. Development. 2016:143:4486–4494. https://doi.org/10.1242/dev.141283.

Pasquesi GIM, et al. Squamate reptiles challenge paradigms of genomic repeat element evolution set by birds and mammals. Nat Commun. 2018:9:2774. https://doi.org/10.1038/s41467-018-05279-1.

Pennock LA. Triploidy in parthenogenetic species of the teiid lizard, genus *Cnemidophorus*. Science. 1965:149:539–540. https://doi.org/10.1126/science.149.3683.539.

Persons TB, Wright JW, Gotte SW. Origin of an Arizona population of the New Mexico Whiptail Lizard (*Aspidoscelis neomexicanus*): evidence from skin grafting and review of an enigmatic specimen. Sonoran Herpetol. 2021:34:70–78.

Pertea G, Pertea M. GFF utilities: GffRead and GffCompare. F1000Res. 2020:9:304. https://doi.org/10.12688/f1000research.23297.2.

Pokorná M, Kratochvíl L. Phylogeny of sex-determining mechanisms in squamate reptiles: are sex chromosomes an evolutionary trap? Zool J Linn Soc. 2009:156:168–183. https://doi.org/10.1111/j.1096-3642.2008.00481.x.

Ramírez F, et al. deepTools2: a next generation web server for deep-sequencing data analysis. Nucleic Acids Res. 2016:44:W160–W165. https://doi.org/10.1093/nar/gkw257.

Ranallo-Benavidez TR, Jaron KS, Schatz MC. GenomeScope 2.0 and Smudgeplot for reference-free profiling of polyploid genomes. Nat Commun. 2020:11:1432. https://doi.org/10.1038/s41467-020-14998-3.

Reeder T, Dessauer HC, Cole CJ. 2002. Phylogenetic relationships of whiptail lizards of the genus Cnemidophorus (Squamata, Teiidae): a test of monophyly, reevaluation of karyotypic evolution, and review of hybrid origins. American Museum Novitates ; no. 3365. Phylogenetic relationships of Cnemidophorus. https://digitallibrary.amnh.org/handle/2246/2854

Rice P, Longden I, Bleasby A. EMBOSS: the European molecular biology open software suite. Trends Genet. 2000:16:276–277. https://doi.org/10.1016/s0168-9525(00)02024-2.

Servant N, et al. HiC-Pro: an optimized and flexible pipeline for Hi-C data processing. Genome Biol. 2015:16:259. https://doi.org/10.1186/s13059-015-0831-x.

Simão FA, Waterhouse RM, Ioannidis P, Kriventseva EV, Zdobnov EM. BUSCO: assessing genome assembly and annotation completeness with single-copy orthologs. Bioinformatics. 2015:31:3210–3212. https://doi.org/10.1093/bioinformatics/btv351.

Simion P, et al. Chromosome-level genome assembly reveals homologous chromosomes and recombination in asexual rotifer *Adineta vaga*. Sci Adv. 2021:7:eabg4216. https://doi.org/10.1126/sciadv.abg4216.

Sites JW, Reeder TW, Wiens JJ. Phylogenetic insights on evolutionary novelties in lizards and snakes: sex, birth, bodies, niches, and venom. Annu Rev Ecol Evol Syst. 2011:42:227–244. https://doi.org/10.1146/annurev-ecolsys-102710-145051.

Smit A, Hubley R. 2008. RepeatModeler Open-1.0. 2008-2015. http://www.repeatmasker.org. http://www.repeatmasker.org

Smit A, Hubley R, Green R. 2008. RepeatMasker Open-4.0. http://www.repeatmasker.org

Smith SD, Pennell MW, Dunn CW, Edwards SV. Phylogenetics is the new genetics (for most of biodiversity). Trends Ecol Evol. 2020:35:415–425. https://doi.org/10.1016/j.tree.2020.01.005.

Spangenberg V, et al. Tendency towards clonality: deviations of meiosis in parthenogenetic Caucasian rock lizards. Biol Reprod. 2025:113:387–396. https://doi.org/10.1093/biolre/ioaf091.

Suryamohan K, et al. The Indian cobra reference genome and transcriptome enables comprehensive identification of venom toxins. Nat Genet. 2020:52:106–117. https://doi.org/10.1038/s41588-019-0559-8.

Tarkhnishvili D, et al. Genotypic similarities among the parthenogenetic Darevskia rock lizards with different hybrid origins. BMC Evol Biol. 2020:20:122. https://doi.org/10.1186/s12862-020-01690-9.

Taylor HL, Cole CJ, Dessauer HC, Parker ED. 2003. Congruent patterns of genetic and morphological variation in the parthenogenetic lizard Aspidoscelis tesselata (Squamata, Teiidae) and the origins of color pattern classes and genotypic clones in eastern New Mexico. American Museum Novitates; no. 3424. http://hdl.handle.net/2246/2789

Tucker AE, Ackerman MS, Eads BD, Xu S, Lynch M. Population-genomic insights into the evolutionary origin and fate of obligately asexual Daphnia pulex. Proc Natl Acad Sci. 2013:110:15740–15745. https://doi.org/10.1073/pnas.1313388110.

Walker JM, Cordes JE, Taylor HL. Parthenogenetic *Cnemidophorus tesselatus* complex (Sauria: Teiidae): a neotype for diploid *C. tesselatus* (Say, 1823), redescription of the taxon, and description of a new triploid species. Herpetologica. 1997:53:233–259.

Waters PD, et al. Microchromosomes are building blocks of bird, reptile, and mammal chromosomes. Proc Natl Acad Sci. 2021:118:e2112494118. https://doi.org/10.1073/pnas.2112494118.

White MJD, Cheney J, Ley KHL. A parthenogenetic species of grasshopper with complex structural heterozygosity (Orthoptera: Acridoidea). Aust J Zool. 1963:11:1–19. https://doi.org/10.1071/zo9630001.

Associate editor: Carina Mugal